Comparison of Ceilometer, Satellite, and Synoptic Measurements of Boundary-Layer Cloudiness and the ECMWF Diagnostic Cloud Parameterization Scheme during ASTEX

CHRISTOPHER S. BRETHERTON

Atmospheric Science Department, University of Washington, Seattle, Washington

E. KLINKER

European Centre for Medium-Range Weather Forecasts, Reading, England

A. K. BETTS

Atmospheric Research, Pittsfield, Vermont

J. A. COAKLEY JR.

College of Oceanic and Atmospheric Sciences, Oregon State University, Corvallis, Oregon

(Manuscript received 26 June 1994, in final form 3 January 1995)

ABSTRACT

Cloud fraction is a widely used parameter for estimating the effects of boundary-layer cloud on radiative transfer. During the Atlantic Stratocumulus Transition Experiment (ASTEX) during June 1992, ceilometer and satellite-based measurements of boundary-layer cloud fraction were made in the subtropical North Atlantic, a region typified by a 1–2 km deep marine boundary layer with cumulus clouds rising into a broken stratocumulus layer underneath an inversion. Both the diurnal cycle and day-to-day variations in low-cloud fraction are examined. It is shown that ECMWF low cloudiness analyses do not correlate with the observed variations in cloudiness and substantially underestimate the mean low cloudiness.

In these analyses, the parameterization of low cloud fraction is primarily based on the inversion strength. A comparison of ECMWF analyses and ASTEX soundings (most of which were assimilated into the analyses) shows that the thermodynamic structure of the boundary layer and the inversion strength are well represented (with some small but significant systematic biases) in the analyses and preserved (again with some biases) in 5-day forecasts.

However, even when applied to the actual sounding the ECMWF low cloud scheme cannot predict the observed day-to-day variations or the diurnal cycle in low cloud. Other diagnostic schemes based on lower tropospheric stability, cloud-top entrainment instability, boundary-layer depth, and vertical motion do equally poorly. The only successful predictor of low cloud fraction from sounding information is the relative humidity in the upper part of the boundary layer.

1. Introduction

Boundary-layer clouds have the largest net impact on the earth's radiation budget of all cloud types (Hartmann et al. 1992). The complex feedbacks between radiation, microphysics, convection, and surface fluxes that maintain these clouds have not proven simple to parameterize. Forecast and climate models must use the simplest possible parameterizations for boundary-layer cloud optical properties, often based on a mean cloud optical depth and cloud fraction over a horizontal grid cell. Since boundary-layer clouds of more than 50-m thickness are nearly optically black and tend to have a large aspect ratio, the cloud fraction is crucial for estimating the effects of broken boundary-layer cloud field on longwave radiative transfer. It is also used in conjunction with the cloud optical depth for parameterizations of shortwave radiative transfer through broken cloud layers. As pointed out by many researchers (e.g., Welch and Wielicki 1985; Stephens 1988; Kobayashi 1993; Cahalan et al. 1994), cloud shape and horizontal inhomogeneity can have significant radiative effects—even for a given mean optical depth and cloud fraction. Nevertheless, it would be a major stride toward modeling the feedbacks between oceanic boundary-layer clouds and climate if we could just predict the latter parameters accurately. At a minimum, this

Corresponding author address: Christopher S. Bretherton, Atmospheric Science Department, Box 351640, University of Washington, Seattle, WA 98195.

requires that (i) the boundary-layer vertical structure is accurately represented in the model and (ii) a skillful parameterization is used for predicting cloud fraction and optical depth, given the boundary-layer structure. These are closely coupled requirements, since the strong radiative feedbacks of boundary-layer clouds imply that a skillful prediction of cloud optical properties should lead to better forecasts of boundary-layer structure.

In the past, both boundary-layer structure and cloud prediction have been serious problems for forecast and climate models. During the 1987 First ISCCP Regional Experiment marine stratocumulus experiment off the coast of California, both ECMWF (European Center for Medium-Range Weather Forecasts) and the National Meteorological Center analyses greatly distorted the observed mean structure of the marine boundary layer (MBL). One major error was a moist bias of several g kg^{-1} above the inversion. A second error was that the observed sharp inversion capping the MBL was replaced in the model analyses by a broad stable layer (Minnis et al. 1992). Since this time, there have been substantial improvements in the vertical resolution of the models and in representation of shallow cumulus and stratocumulus convection (Tiedtke 1989). These should result in better first-guess fields, which are a key input into the analyses in data-sparse marine regions.

The parameterization of MBL cloud properties is still a thorny problem. Most forecast and climate models use the Slingo (1987) scheme (see section 2d), which diagnoses boundary-layer cloud fraction based on the inversion strength. Recently, several groups have started implementing prognostic schemes for cloud liquid water and cloud fraction (Smith 1990; Li and Le Treut 1992; Tiedtke 1993). Many, but not all, of the diagnostic and prognostic schemes lead to a severe underestimate of stratocumulus cloud cover in the eastern subtropical oceans when used as part of a climate simulation. The shallow cloud components of these schemes have not been adequately tested against a regional experiment in which both the MBL structure and cloud properties have been measured.

The Atlantic Stratocumulus Transition Experiment (ASTEX) took place during June 1992 in the subtropical North Atlantic, a region typified by a 1–2-km-deep boundary layer with cumulus clouds rising into a broken stratocumulus layer underneath an inversion (Albrecht et al. 1995). A variety of measurements of boundary-layer structure and cloud optical properties were made. To provide accurate regional analyses of mean vertical motion and MBL vertical structure, an effort was made to assimilate the special soundings taken during ASTEX into the ECMWF operational model to augment the very sparse routinely collected upper-air data in this region.

In this paper we first compare three measures of cloud fraction made during ASTEX: ceilometer data, synoptic cloud reports, and retrievals from polar-orbiting satellites (sections 2a,b). We then document both the diurnal cycle and synoptic-scale variability of cloudiness in the ASTEX region (section 2c). We compare these results with analyses of cloudiness from the ECMWF model, which used the Slingo scheme (section 2d). We must next identify whether differences between the modeled and observed cloudiness are due primarily to differences between the analyses and the observed soundings or to problems with the cloudiness parameterization. In section 3a we compare temperature and moisture soundings synthesized from the ECMWF analyses with observed soundings. We also examine systematic errors in MBL vertical structure that develop during forecasts (section 3b). Such errors affect the analyses because earlier forecasts serve as the first guess for an analysis. In addition, an analysis of these errors can reveal problems with the model physical parameterizations, including cloud–radiation interaction and shallow cumulus parameterization. In section 4, we examine the skill of the Slingo scheme and a variety of other proposed diagnostic predictors for deducing daily average cloudiness given the true sounding. Section 5 presents the conclusions.

2. Cloudiness observations during ASTEX

a. Data sources

Three types of cloudiness observation, ceilometers, routine synoptic reports, and satellite retrievals, were used for this study. Time series of low cloud fraction were compiled from laser ceilometers based on two islands—Santa Maria, in the Azores, (SM; 37°N, 25°W; 4–23 June 1992) and Porto Santo, in the Madeira Islands, (PS; 33°N, 16°W; 1–25 June 1992)—and for a third ceilometer aboard the R/V *Valdivia* (VL) for 6–15 June 1992, at which time it was stationed at point P3 (28°N, 24°W). Together these three sites composed the three vertices of the "ASTEX triangle." The SM and VL ceilometer detected cloud bases between 0 and 3.5 km, and a lowest cloud base was reported every 30 s. The PS ceilometer detected cloud bases up to 10 km (i.e., including cirrus), with one observation every 60 s. Only clouds with bases below 2.4 km were classified as low cloud. The frequency of cloud base in each of 12 bins (0–200 m, 200–400 m, . . . , 2200–2400 m, >2400 m) and the overall low cloud fraction were tabulated for each hour. Routine hourly synoptic reports (synops) of low cloudiness in oktas were also obtained from the *Valdivia.*

Total cloud fraction and cloud-top temperature of the highest cloud layer were retrieved twice a day during June 1992 on a 2° × 2° grid from *NOAA-12* (overpass at within an hour of 0930 UTC) and *NOAA-11* (within an hour or so of 1600 UTC) polar-orbiter satellite imagery, using the method of Coakley and Bretherton (1982). Some passes (8, 22, 25, 26, 28 June for *NOAA-11;* 7, 12, 14, 18, 26 June for *NOAA-12*) could not be

analyzed because of an unfavorable viewing angle. The ASTEX region often included cirrus as well as low-lying cloud, and we estimate that the mean total cloud fraction exceeded the mean low cloud fraction by 0.1–0.2. Many retrieved cloud-top temperatures were between 265 and 275 K, which was below the 280–285 K typically found in soundings at the trade inversion base (see section 2) and was not supported by the low relative humidities typically found in the 265–275-K temperature range in the soundings. This may reflect a calibration problem or contamination by thin cirrus. Detectable cirrus was also common. We classified 2° × 2° boxes with cloud tops with retrieved temperatures above 265 K as free of satellite-detected high cloud and interpreted the cloud fraction in these boxes as due to low cloud.

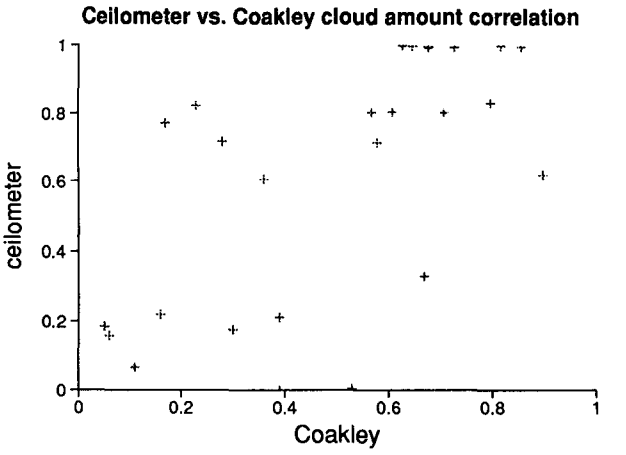

FIG. 2. Scatterplot of satellite-derived cloud fraction vs ceilometer cloud fraction at Porto Santo.

b. *Cloud data intercomparison*

We intercompared these three types of data at the three ceilometer sites. The 3-h average ceilometer cloud amounts from the *Valdivia* were well correlated with the average of the 3-h synops, though the synops were typically 20% higher (Fig. 1). This bias is expected since the ceilometer measures zenith cloud fraction, while the observer reports a whole-sky cloud fraction, which will be larger except for clouds whose height is much less than their width.

Satellite-derived cloudiness interpolated to the surface site was also correlated with the ceilometer data at all three sites. At PS, the ceilometer could detect all clouds with a definable base and could directly be compared to total cloud cover. At all three sites we have compared satellite and ceilometer low cloud cover for passes in which there was no satellite-detected high cloud. Little bias between satellite and ceilometer cloud fractions was observed (Fig. 2). However, the correlation was less than 0.5. The ceilometer cloudiness is averaged over the 3-h period, including the satellite pass. With 7 m s^{-1} winds, even a 3-h averaging time corresponds to a downstream distance of only 70 km. Satellite images show large inhomogeneity in cloud properties on this scale. This inhomogeneity was filtered by the satellite-derived cloud fraction, since it was based on a much larger averaging area of $O(200$ km) on a side.

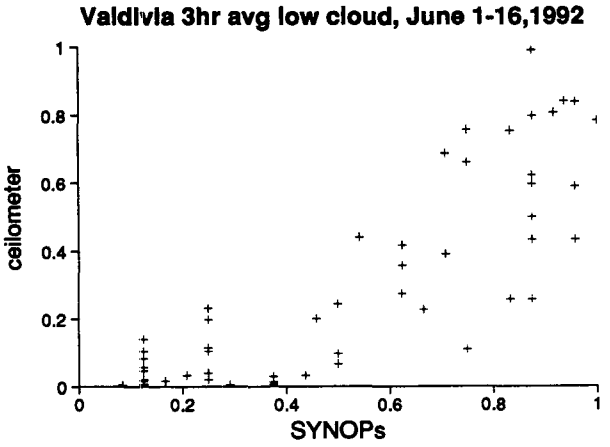

FIG. 1. The 3-h average synop vs ceilometer cloud fraction from the *Valdivia*, 1–16 June.

c. *Climatology and diurnal cycle of cloud in ASTEX*

As documented by Albrecht et al. (1995), typical MBL cloud cover during ASTEX consisted of scattered clusters of cumulus clouds with bases between 950 and 1000 hPa, rising into a patchy 50–300 m thick stratocumulus layer responsible for most of the areal coverage by cloud. The top of the stratocumulus clouds generally coincided with a sharp trade inversion of 2–8 K at a pressure of 800–900 hPa. Figure 3 shows mean total cloud cover for the morning and for the afternoon, based on the available satellite passes between 1 and 23 June. We excluded from these means the period from 24 June onward, during which a strong midlatitude frontal system swept through the triangle from the northwest and set up a rather uncharacteristic cloud regime. Over the entire ASTEX triangle, total cloudiness was between 0.4 and 0.7 at 0930 UTC, with a 0.05–0.2 decrease in the afternoon pass.

Ceilometer observations give a more complete view of the diurnal cycle (Fig. 4). The mean low cloudiness was 68% at SM, 52% at PS, and 40% at P3. All three sites had minimum cloud at 1500 UTC and maximum cloud fraction at 0600–0700 UTC. (Note that true solar noon occurs close to 1300 UTC at PS and 1340 UTC at SM and P3.) The ceilometer measurements suggest that the two satellite passes at 0930 and 1600 UTC do not capture the full diurnal range and that low cloud cover at 0930 UTC is near to the daily average. The

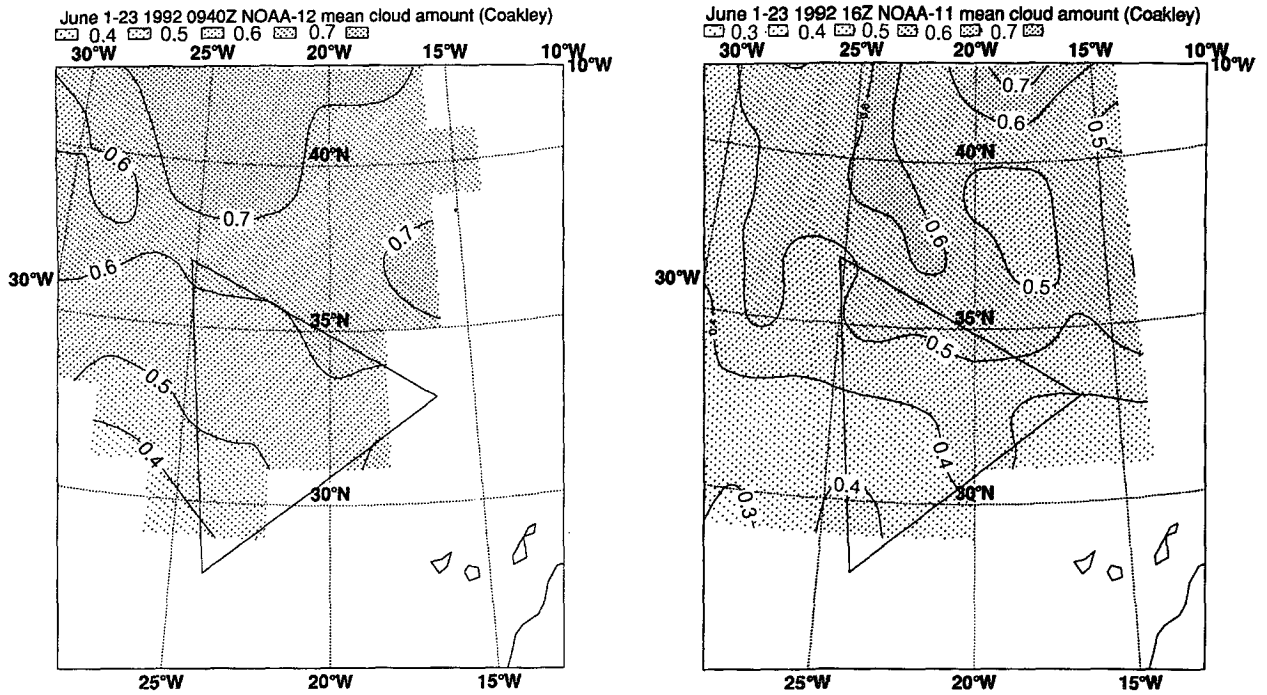

FIG. 3. The 1–23 June mean total cloud cover from polar orbiter retrievals at (a) about 0930 and (b) about 1600 UTC.

peak-to-peak diurnal range in cloud fraction was substantial—0.2 at SM, 0.25 at PS, and over 0.4 at P3. The 9-day period for which the *Valdivia* ceilometer was operational at P3 was a period of exceptionally steady inversion height, perhaps isolating the diurnal cycle in a particularly pure form. However, this period may have been too short to be representative.

Rozendaal et al. (1994) examined global patterns in the diurnal cycle of low cloud from International Satellite Cloud Climatology Project (ISCCP) satellite retrievals and surface observer reports. They found a mean diurnal cycle of 16%–20% peak-to-peak amplitude in June–August cloud fraction near P3 (28°N, 24°W), with maximum cloudiness 4 h after midnight. While the ISCCP diurnal cycle amplitude is not as large as was observed by the *Valdivia,* it is particularly large in this region, and the phase of the ISCCP diurnal cycle agrees with the *Valdivia* observations. The ISCCP data show that other transitional zones between stratocumulus and trade cumulus also have large diurnal cycles in low cloud fraction.

The open circles for PS and P3 show cloud fraction with cloud base at less than 800 m. Inspection of the data showed that this height was usually above the surface-lifted condensation level but below the base of stratiform cloud. We interpret it qualitatively as a measure of cumulus cloud fraction. The hourly frequency of cloud bases in different height bins did not usually show a clean bimodal distribution, so this measure of cumulus cloud should not be regarded as a quantitative cumulus cloud fraction. At PS, the "cumulus" fraction had little discernible diurnal cycle and was 20%–30% throughout the day. Since the ceilometer site was on the upwind side of the island, the cumulus fraction may have been enhanced, as air lifts up over the island, and may also have responded to the diurnal cycle of island heating. The stratocumulus clouds, which had larger areal extent and a much longer typical lifetime, appear to have been much less affected by the islands. At P3, the cumulus fraction was much smaller and maximized at nighttime in phase with the stratocumulus. We speculate that the strong diurnal cycle at P3 is produced by both a diurnal variation in the flux of liquid water detrained by cumulus clouds into the overlying stratocumulus layer and also the vulnerability of the thin stratocumulus layers seen in the ASTEX region to evaporation by direct solar heating.

Figure 5 shows the daily averaged cloud amount at the three ceilometer sites. At SM there was sizable day-to-day (synoptic) variability in cloud fraction, while at P3, which was in the heart of the trade wind belt, there was much less day-to-day cloudiness variability. In fact, the overall variance in the time series of hourly cloud fraction was comparable at all three sites, but at SM the synoptic variance explained 54% of the overall variance, and the diurnal cycle explained 3%, while at P3 13% of the variance was synoptic and 25% was diurnal; PS was intermediate, with 24% synoptic and 5% diurnal variance fractions. The remainder of the variance in cloudiness was due to irregular short-period

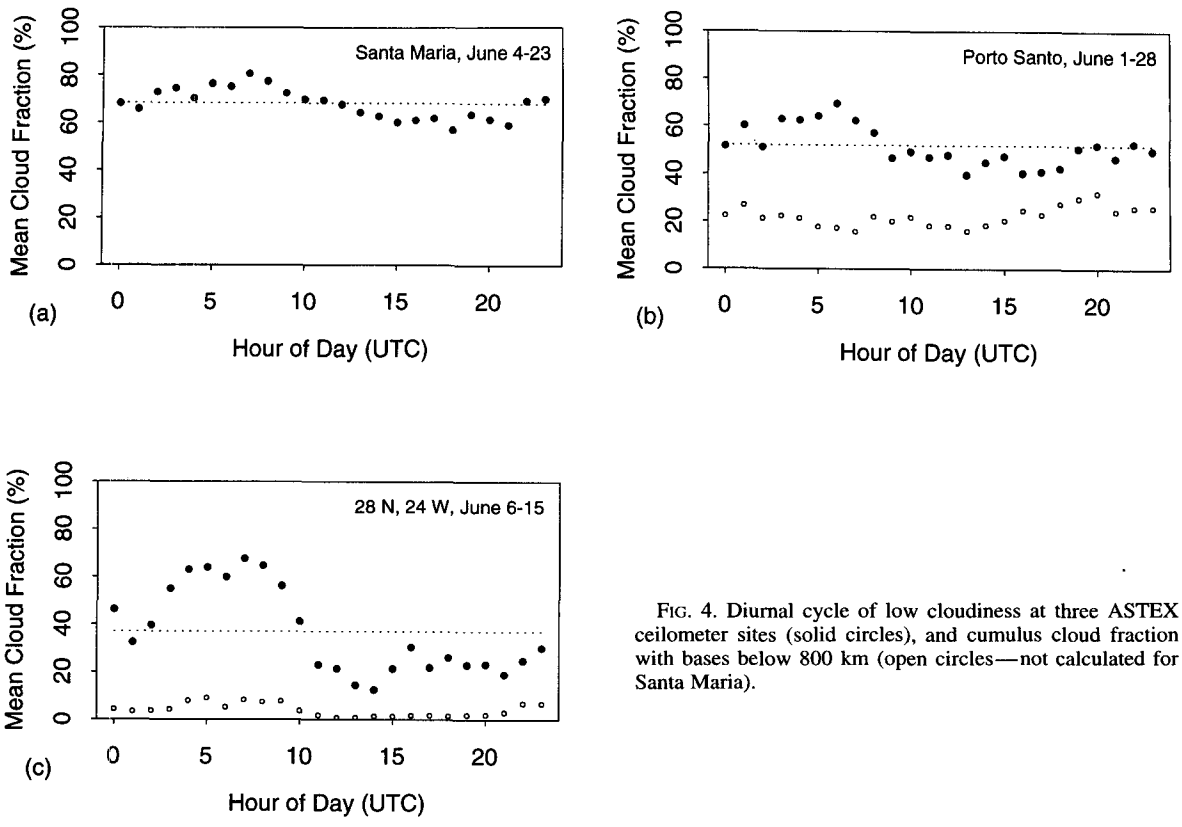

FIG. 4. Diurnal cycle of low cloudiness at three ASTEX ceilometer sites (solid circles), and cumulus cloud fraction with bases below 800 km (open circles—not calculated for Santa Maria).

variability in cloud fraction, probably connected in part to the 20–100 km wide mesoscale patchiness seen in satellite images of the stratocumulus clouds in the ASTEX region.

d. *ECMWF cloudiness analyses*

Cloud properties were diagnosed using cycle 44 of the ECMWF model, which differed negligibly in its boundary-layer and cloud physics from cycle 46, the operational model at the time of ASTEX. Cycle 44 of the ECMWF model incorporated a modified Slingo (1987) scheme for cloudiness parameterization. Cloud was subdivided into low, middle, high, and convective cloud. Convective cloud cover was determined from the convective precipitation rate determined by the cumulus parameterization scheme and was negligible in the ASTEX region. Low cloud was defined to lie below $\sigma = 0.8$ (approximately 820 hPa). Low cloud fraction C_L was assumed to be due to either mean lifting of high relative humidity air or the presence of an inversion capping a moist boundary layer (ECMWF 1991, section 2.5.2):

$$C_L = \max(a_\omega C_{LI}, a_i C_{Li}), \tag{1}$$

$$C_{LI}(p) = [\max\{(RH - 0.7)/0.3, 0\}]^2,$$

$$a_\omega = r(\omega/\omega_c), \quad \omega_c = -0.1 \text{ Pa s}^{-1}, \tag{2}$$

$$C_{Li}(p_i^-) = r(10(\Delta\theta/\Delta p)_{\max} - 0.9),$$

$$a_i = r(\{RH^- - 0.5/0.2\}). \tag{3}$$

Here, $r(x)$ is the ramp function such that $r(x) = 0$ for $x \leq 0$, x for $0 < x < 1$, and 1 for $x \geq 1$. The lifting cloudiness C_{LI} requires mean ascent and occurs in all lifted air with relative humidity $RH > 0.7$.

Time series of ECMWF-analyzed cloudiness at the ASTEX sites did reveal some lifting cloudiness, but most of the cloudiness was inversion cloudiness C_{Li}. This cloud type is assumed to form under capping inversions. The capping inversion strength is diagnosed as the maximum mean stratification $\Delta\theta/\Delta p$ of potential temperature between two successive model levels. [Δp (hPa) is the pressure spacing between the levels.] Only if $(\Delta\theta/\Delta p)_{\max} > 9$ K/(100 hPa) is inversion cloud assumed to form. The relative humidity RH^- is calculated at the model level at the base of the inversion. For relative humidities $RH^- < 0.7$ (a rare situation in ASTEX), inversion cloud is decreased. In summary, for ASTEX $C_L \approx C_{Li}$.

Cloud optical properties are then deduced by assuming a liquid water content equal to 5% of the saturation

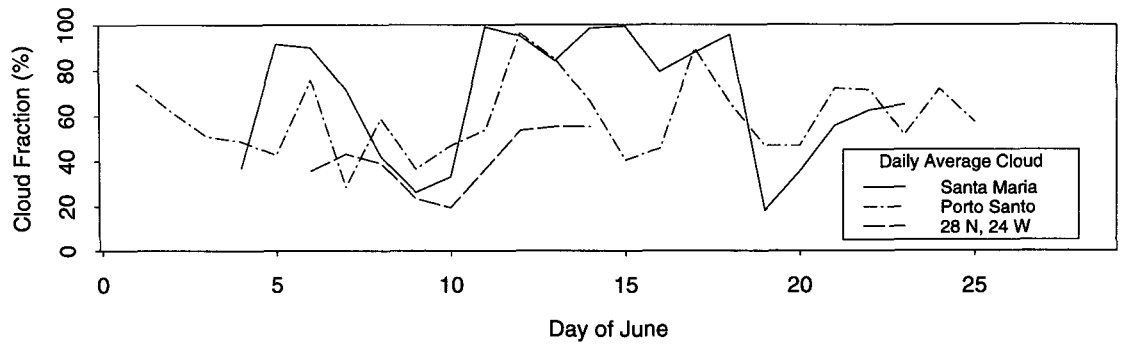

FIG. 5. Time series of daily average ceilometer cloud fraction at the ASTEX sites.

mixing ratio throughout the layer and a pressure-dependent effective radius equal to 15 μm at 850 hPa. Both of these are somewhat high values for subtropical MBL stratocumulus.

Low cloudiness diagnosed in the ECMWF analyses had no detectable correlation with 3-h or daily average ceilometer cloudiness. Figure 6 compares the two at PS. In addition to the lack of correlation, the average ECMWF low cloudiness (Fig. 7a) at PS (0.26) is only half of the ceilometer-observed mean low cloudiness (0.52) at PS. This bias is also seen in mean maps of ECMWF-analyzed total cloudiness over the ASTEX region, which show total cloudiness of between 0.3 and 0.5 over the ASTEX region (Fig. 7), compared to 0.5–0.7 seen from the satellite climatology in Fig. 3a. Because the ECMWF low cloud fraction is determined by inversion strength rather than radiatively driven processes in the MBL, it is no surprise that the diurnal cycle in the ECMWF low cloud cover was weak and highly location dependent in the ASTEX region (Fig. 8). While a layer with $(\Delta\theta/\Delta p)_{\max} > 9$ K/(100 hPa) was almost always seen in the radiosonde soundings,

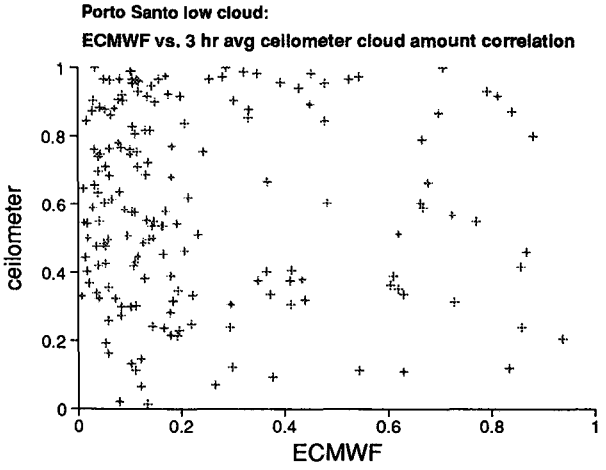

FIG. 6. Scatterplot of ECMWF low cloud fraction vs ceilometer low cloud fraction at Porto Santo.

the ECMWF analysis systematically underestimated $(\Delta\theta/\Delta p)_{\max}$ (section 3), so that there was often little or no diagnosed inversion cloud.

3. Sounding intercomparison

a. Statistical comparison of soundings with ECMWF analyses

A primary goal of the ASTEX experiment was to define as accurately as possible the large-scale environment in which field observations were being taken. The strategy was to incorporate the special upper-air soundings taken during ASTEX into routine ECMWF operational analyses (see Albrecht et al. 1995 for more detail). The operational data assimilation capability of a numerical weather prediction model was an attractive way to integrate ASTEX sounding data with the wealth of information provided by the routine global observing system. Through close collaboration with the Portuguese meteorological research agency INMG and ECMWF, the special soundings were correctly formatted and sent via modem to Lisbon, where they were entered into the Global Telecommunications System (GTS) and incorporated into the operational ECMWF model.

Cycle 44 of the ECMWF model used only wind, geopotential height, and relative humidity information from the standard operational pressure levels (1000, 850, 700, ... hPa) of the soundings. Temperatures were calculated based on pressure thicknesses. Due to the very coarse vertical resolution of these data, the initial guess from the forecast model was crucial in filling in much of the vertical detail of MBL structure in the analyses. Of the model's 31 vertical σ levels, 9 are between the surface and 700 hPa. For a surface pressure of 1011.2 hPa, these levels are at pressures of 1011, 997, 973, 941, 904, 863, 819, 773, and 727 hPa, giving the model a 30–45 hPa vertical resolution through most of the MBL. For comparison with the sounding data, the ECMWF analyses were vertically interpolated to constant pressure levels with a vertical spacing of 25 hPa. Except in the surface layer, this vertical spacing

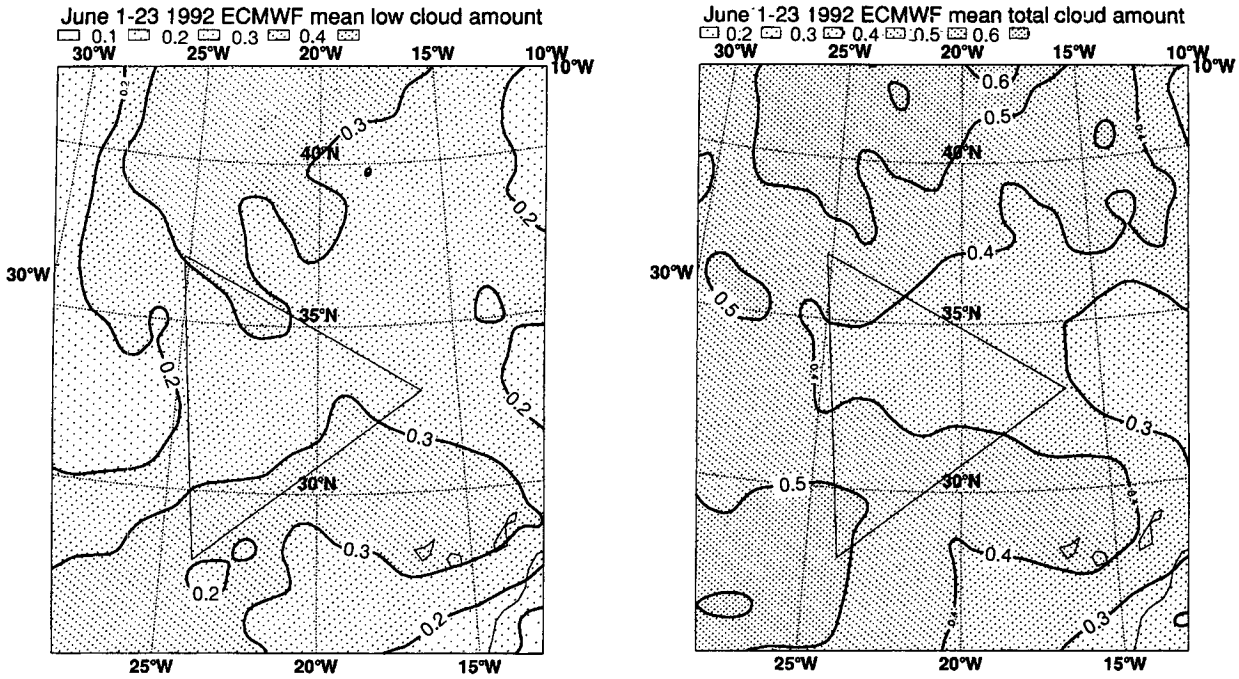

FIG. 7. The 1–23 June mean ECMWF (a) low cloud cover and (b) total cloud cover.

is less than the model resolution, so the implicit smoothing due to this interpolation was negligible. The soundings were averaged over 25-hPa pressure intervals for the comparison. Since the assimilation only tries to match the analyses and observations at 150-hPa vertical resolution, comparison of the soundings and ECMWF analyses at 25-hPa resolution can show whether the detailed MBL vertical structure inherited by the analyses from the model first-guess fields was systematically different than the detailed vertical structure in the soundings.

Table 1 summarizes the sounding statistics for all sounding platforms. The 3-h soundings were taken from 1 to 26 June at SM and PS and were also made at P3 (the third vertex of the ASTEX triangle) from 1 to 15 June from the R/V *Valdivia* and from 22 to 28 June from the R/V *Malcolm Baldridge*. In addition, the R/V *Le Suroit,* usually stationed within 200 km south or east of Santa Maria, took 6-h soundings from 1 to 20 June. Almost all of the above soundings were entered into the GTS. Before 23 June, the R/V *Oceanus* and the R/V *Malcolm Baldridge* took sporadic soundings from a variety of locations, most of which were not entered into the GTS. Overall, over 75% of the 788 special soundings taken from two islands and four ships during ASTEX were put on to the GTS before the ECMWF data cutoff of 7 h after the nominal observation time. Only a few soundings were rejected by

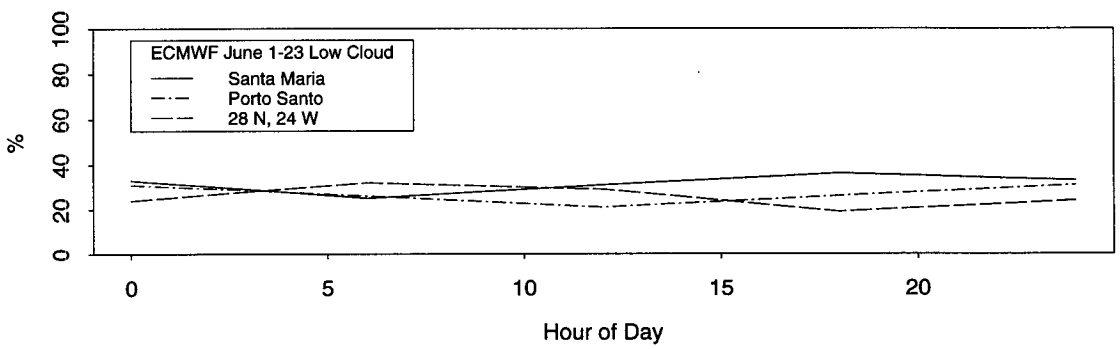

FIG. 8. The mean diurnal cycle of low cloud fraction from 1 to 23 June 6-h forecasts for 0000, 0600, 1200, and 1800 UTC.

TABLE 1. ASTEX sounding sites.

Location	Lat/Lon	Dates	Per day	Total	GTS	Ceilometer
Santa Maria	37°N, 25°W	1–27 June	8	190	183	4–26 June
Porto Santo	33°N, 16°W	1–27 June	8	198	187	1–25 June
R/V *Valdivia*	28°N, 24°W	1–17 June	8	117	98	6–17 June
R/V *Le Suroit*	Variable, up to 200 km south and east of SM.	1–20 June	4	72	60	No
R/V *Oceanus*	Variable, north of ASTEX triangle.	3–23 June	Irregular	76	10	No
R/V *Malcolm Baldridge*	Variable, at 28°N, 24°W on 22–28 June.	7–27 June	Irregular	135	58	Yes

ECMWF quality control software, except during 1–12 June when all soundings at SM were rejected because the ECMWF database had not been given the correct station elevation.

We compared soundings extracted from initialized analyses from the ECMWF model with the ASTEX soundings. A typical sounding from Porto Santo (Fig. 9) shows that, remarkably, the analysis retained the essential features of the sounding in and above the MBL, despite using only standard-level data. A statistical comparison of actual and ECMWF-derived soundings was carried out for all ASTEX sounding sites. Figure 10 shows this comparison for 1–27 June for Porto Santo. This site was characterized by moderate synoptic-scale variability, as seen in the 2 K standard deviations of potential temperature θ and the 2 g kg^{-1} standard deviation of mixing ratio q_v from their monthly mean at the 850-hPa mean inversion height. The ECMWF analyses captured the synoptic variability quite well. The correlations between time variations in the analyzed and observed temperature and mixing ratio were up to 0.9 in the free troposphere and above 0.5 at all levels.

The ECMWF analyses had a 1 g kg^{-1} dry and a 0.5-K warm bias in the cloud layer at 900 hPa. Above the

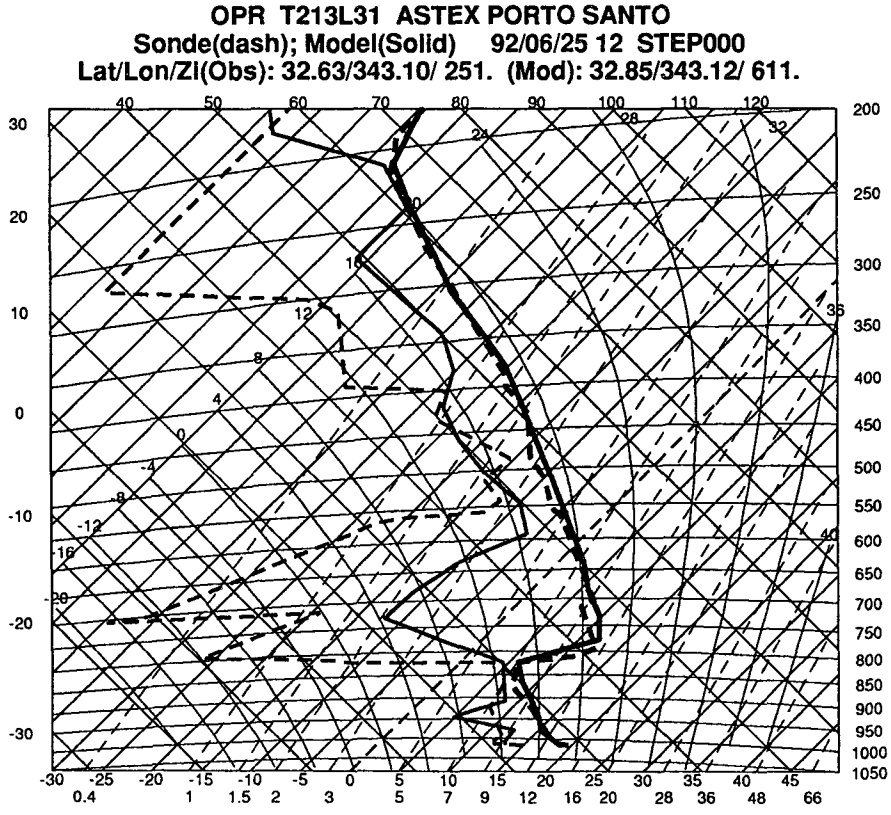

FIG. 9. Tephigram of temperature and dewpoint for 25 June 1992 at Porto Santo from ECMWF analysis (solid) and radiosonde (dashed).

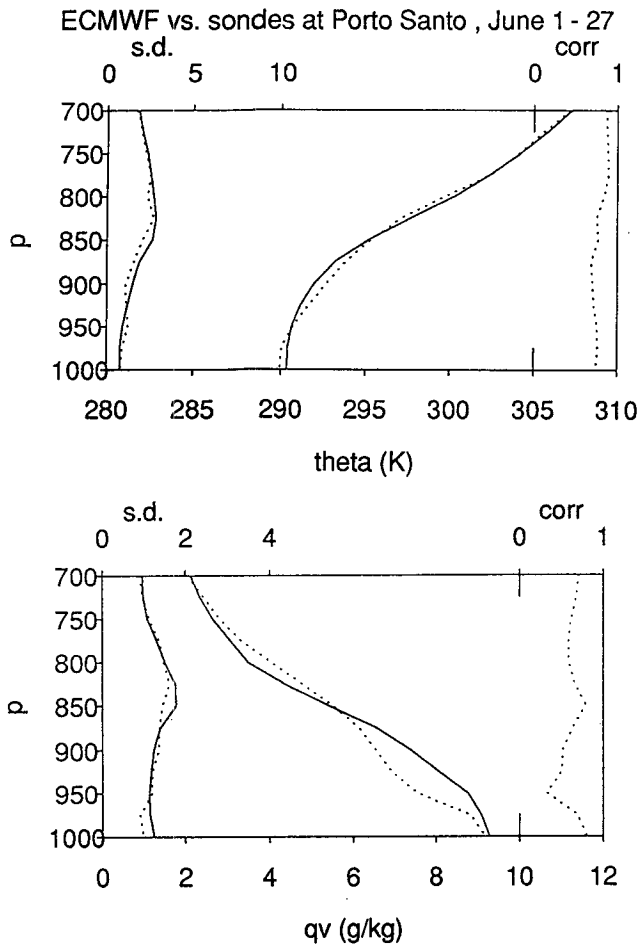

FIG. 10. The 1–28 June Porto Santo mean soundings of θ and q_v. For each panel solid lines denote sondes, dotted lines are ECMWF. The lines at left are standard deviations and the line at right is the sonde–ECMWF correlation.

mean inversion the bias was reversed. Qualitatively, the effect was to smear out the inversion in the analyses. These systematic errors were substantially smaller than the standard deviations in θ and q_v, due to synoptic-scale variability, but they were consistently found at all six sounding sites. Hence, they are unlikely to be an island effect. The wind components showed small and site-dependent biases.

Three implications of the thermodynamic biases follow:

1) The relative humidity in the upper part of the MBL was 5%–10% too dry in the ECMWF analysis, while above the inversion it was 5% too moist.

2) The analyzed inversion tended to be slightly too weak. The ECMWF parameterization [Eq. (3)] of inversion cloud is very sensitive to this error; a 1-K underestimate of the potential temperature change $\Delta\theta$ through a 40-hPa deep layer including the inversion causes a 25% decrease in predicted low cloud cover.

3) The ECMWF MBL was less conditionally unstable than observed. The *Valdivia* soundings from 7 to 14 June are a particularly good comparison, since vertical smoothing due to synoptic variability was small, there were consistently eight soundings a day, and there was no possible contamination by island effects.

Figure 11 shows the mean observed and ECMWF soundings for this period. The observed sounding has been interpolated to 25-hPa vertical resolution for a fairer comparison with the ECMWF model vertical resolution. The observed mean sounding was conditionally unstable to the lifting of air from 1000 hPa (and even more so to the lifting of surface air), but the ECMWF mean sounding is not. In fact, a 7–14 June 3-h time series (not shown) of the convective available potential energy (CAPE) of air lifted from 1000 hPa shows that only 16% of the ECMWF soundings had positive CAPE, while 77% of the radiosonde soundings had positive CAPE.

b. Systematic model biases

One (though by no means the only) source of analysis biases is systematic errors in short-range ECMWF forecasts, which we analyze following a technique of Klinker and Sardeshmukh (1992). A 7-h global forecast using cycle 44 of the model at T106 horizontal resolution was initialized from each 6-h analysis. Figure 12 shows the heat budget for the second hour of the forecast as a function of latitude averaged over a 10° wide zonal strip in the ASTEX region. The monthly average of the temperature tendency was negligibly small. Hence, the residual (Fig. 12c)—after adding the "adiabatic" tendency (Fig. 12a) due purely to advection with the "diabatic" tendency (Fig. 12b) due to physical parameterization schemes—is what drove systematic forecast errors. The adiabatic tendencies mainly reflected subsidence warming and reached maximum values of up to 2.8 K day^{-1} in the boundary layer. In the lower part of the MBL, horizontal cold advection dominated to produce an adiabatic cooling tendency of 1–2 K day^{-1}. The diabatic tendencies were roughly opposite. In and above the trade inversion they were dominated by radiative cooling (Fig. 12d), while transport of heat by cumulus convection (Fig. 12e) and vertical diffusion (Fig. 12f) were also important within the MBL. There was a residual cooling at all heights in the MBL, rising from near zero at the surface to maximum values of 0.8 K day^{-1} in the trade inversion. This cooling caused a systematic rise of the trade inversion in longer forecasts.

The corresponding budget of specific humidity is shown in Fig. 13. There was weak residual drying of 0.1 g kg^{-1} day^{-1} in the trade inversion, and a large residual moistening of approximately 1 g kg^{-1} day^{-1} in the near-surface layer. Assuming that the errors in the adiabatic processes were comparatively small, this suggests that either the surface latent heat flux was too

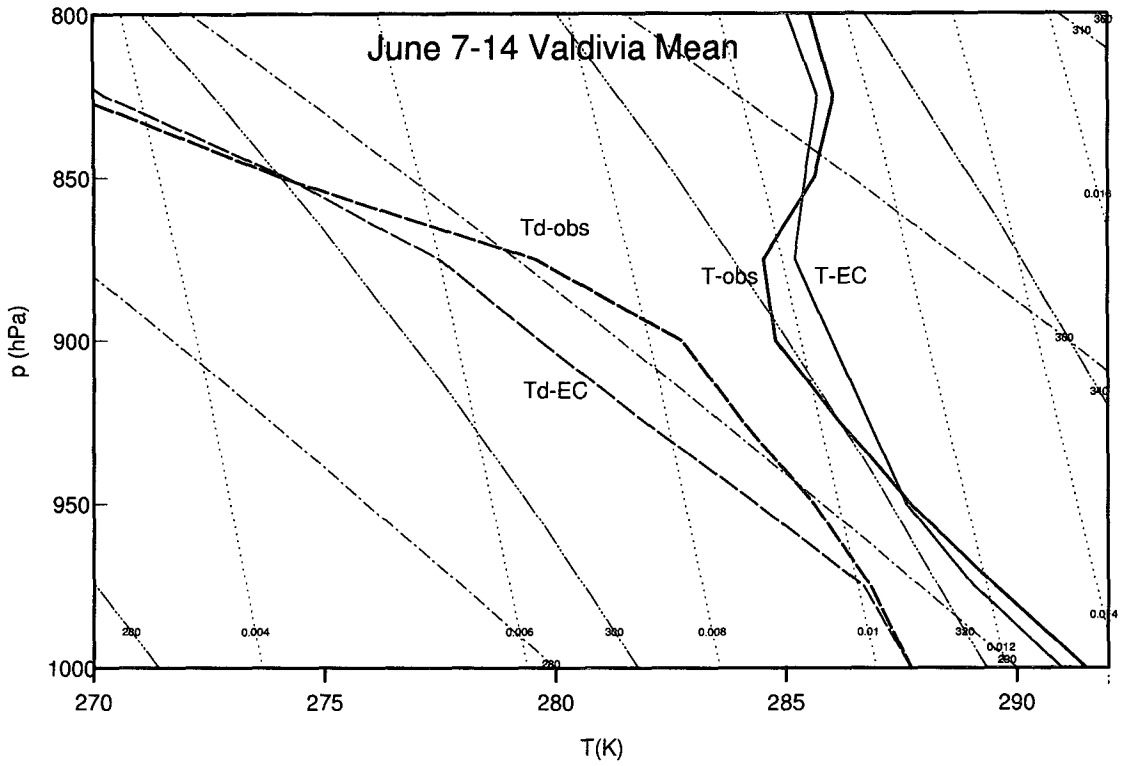

FIG. 11. The 6–14 June mean soundings from the *Valdivia* (thick) and ECMWF analyses (thin). Solid curves indicate temperature; long dashes indicate dewpoint temperature. Dotted, dot–dash, and triple-dot–dash lines are isopleths of mixing ratio, potential temperature, and equivalent potential temperature, respectively.

large by 10 W m^{-2} in the model or that the shallow convection was not efficient enough to transport moisture upward into higher levels of the MBL or some combination of these effects. The fact that the residual was localized to the lowest model levels, principally because cumulus drying (Fig. 13d) was not keeping up with upward vertical moisture diffusion (Fig. 13e), implicates inefficient vertical mixing processes, but we note that poor vertical mixing alone cannot explain why there was net vertically integrated moistening averaged over the depth of the MBL.

As pointed out in the previous section, there was often little or no CAPE in the ECMWF-analyzed MBL. Thus, in the first few timesteps of a forecast we expect little shallow convection, so moisture cannot be mixed out of the subcloud layer. However, at the same time cumulus cooling in the upper part of the MBL is initially weak. Were cumulus convection strong enough to mix out the surface moisture, the residual cooling in the upper part of the MBL, already negative, would be even stronger. The most obvious explanation for the temperature residual is excessive radiational cooling near the inversion, but at the same time low cloud fraction (which should augment the cooling) was severely underpredicted.

These biases were also apparent when the daily operational 1- and 5-day forecast were compared to the analyses during June 1992 in the ASTEX region. The 1-day mean forecast temperature error (Fig. 14a) was very similar to the residual temperature tendency, and by day 5 (Fig. 14b) the error magnified by a factor of 2 in the lower troposphere (and more aloft), corresponding to a 30-hPa rise in mean inversion height and a 1.3-K strengthening of the inversion during the forecast. The structure of the humidity errors in the 1-day forecast (Fig. 15a) was similar to the humidity residual field, with up to 0.6 g kg^{-1} moistening in the lowest levels. By day 5, the errors in the upper part of the MBL above the lifted condensation level of surface air increased somewhat, but the surface errors did not increase (Fig. 15b), perhaps because during the first day the sounding destabilized sufficiently to produce more convective mixing of moisture out of the surface layers.

Some of the error growth may have involved feedbacks involving cloud–convection–radiation interaction. In the forecasts, if there is initially net cooling at the inversion, the trade inversion strengthens, more low cloud forms, and the radiative cooling at the inversion intensifies. This feedback could amplify the effect of

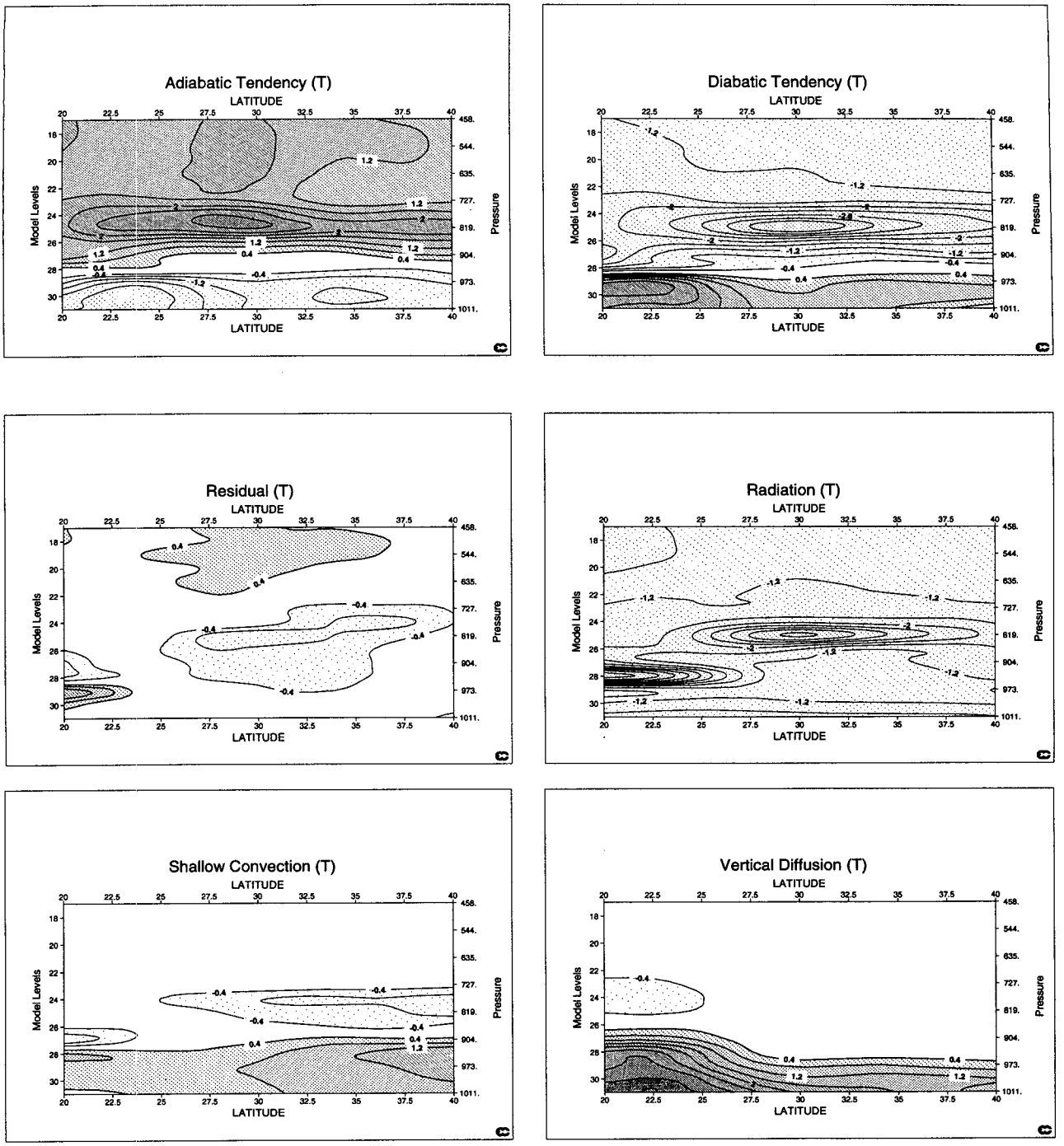

FIG. 12. Vertical cross sections of the heat budget for June 1992, zonally averaged between 25°W and 15°W. The tendencies are month-long averages over the first and second hours of ECMWF forecasts run four times a day: (a) adiabatic tendencies, (b) diabatic tendencies, (c) residual, (d) radiation, (e) cumulus condensation, and (f) vertical diffusion. Note that the tendencies are plotted as a function of model level and do not correspond to uniform spacing in pressure.

any initial imbalance in the heat budget. In fact, this feedback created a 5% average increase in low cloud over most of the ASTEX region over the course of a 5-day forecast.

It is a bit surprising that the analysis biases were somewhat different than the forecast biases. The "smearing" of the inversion seen in the analyses was not seen in the 1-day forecast, nor was the strong sur-

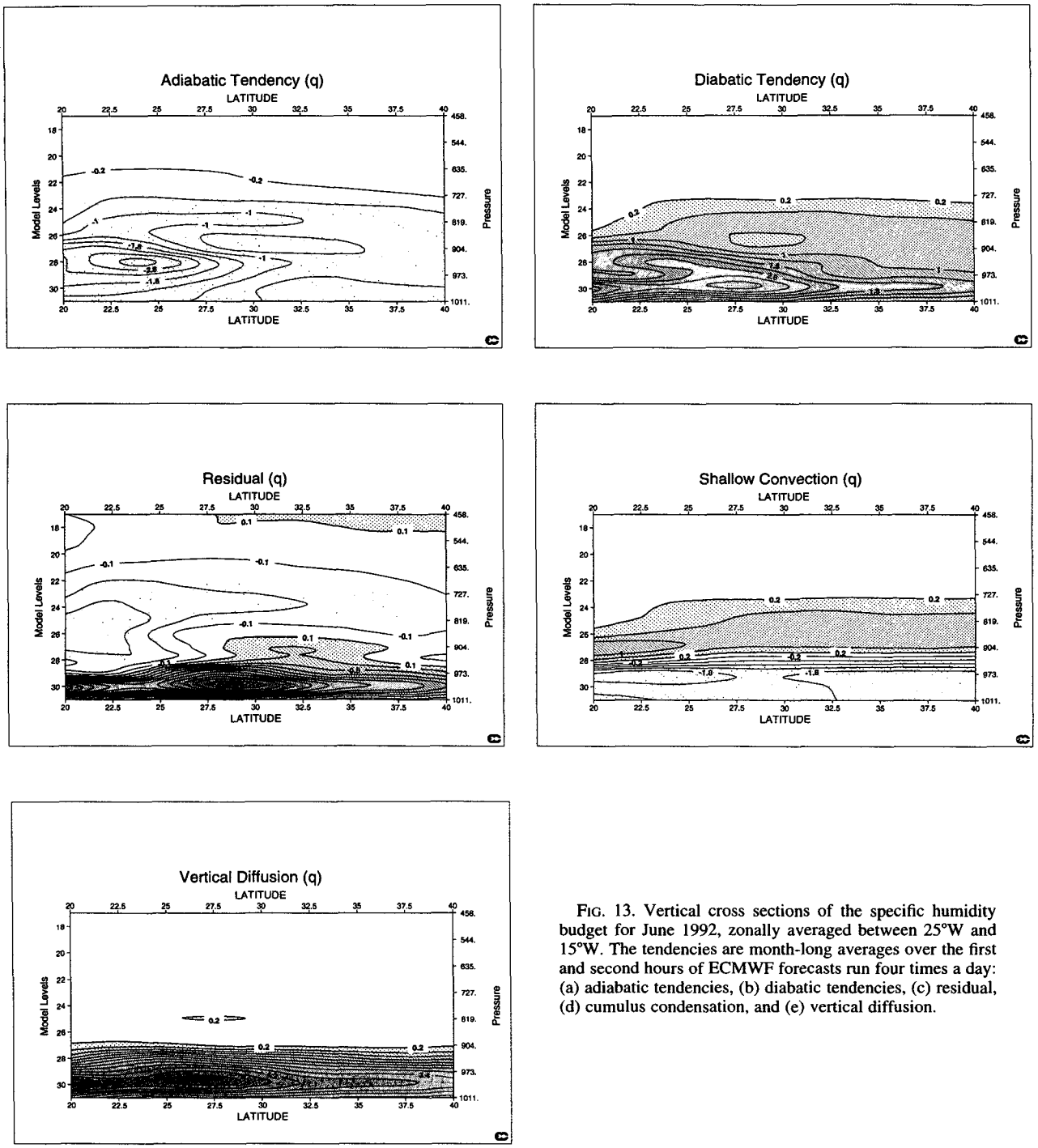

FIG. 13. Vertical cross sections of the specific humidity budget for June 1992, zonally averaged between 25°W and 15°W. The tendencies are month-long averages over the first and second hours of ECMWF forecasts run four times a day: (a) adiabatic tendencies, (b) diabatic tendencies, (c) residual, (d) cumulus condensation, and (e) vertical diffusion.

face moistening seen in the 1-day forecast seen in the analyses. It may be that the forecasts were sufficiently free of systematic error that the analysis biases had more to do with how initial guess and observations are combined to produce an initialized analysis than with the forecast errors per se.

4. Cloudiness parameterizations applied to the ASTEX soundings

a. The Slingo parameterization

In section 2, we found that the ECMWF low cloud had little correlation with ceilometer observations, even

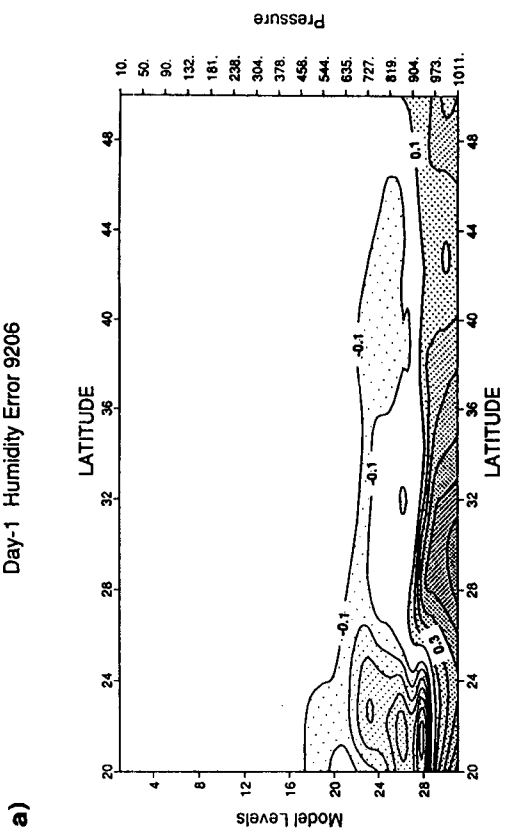

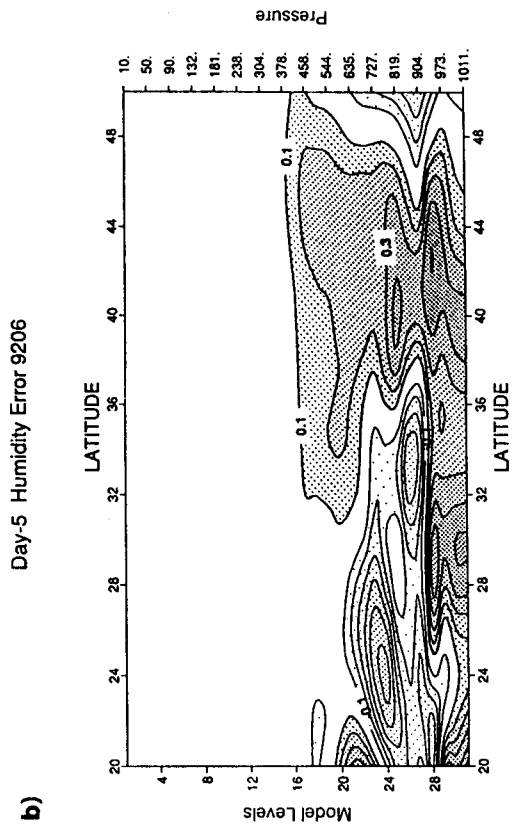

FIG. 15. Monthly (a) day 1 and (b) day 5 mean forecast humidity errors for June 1992.

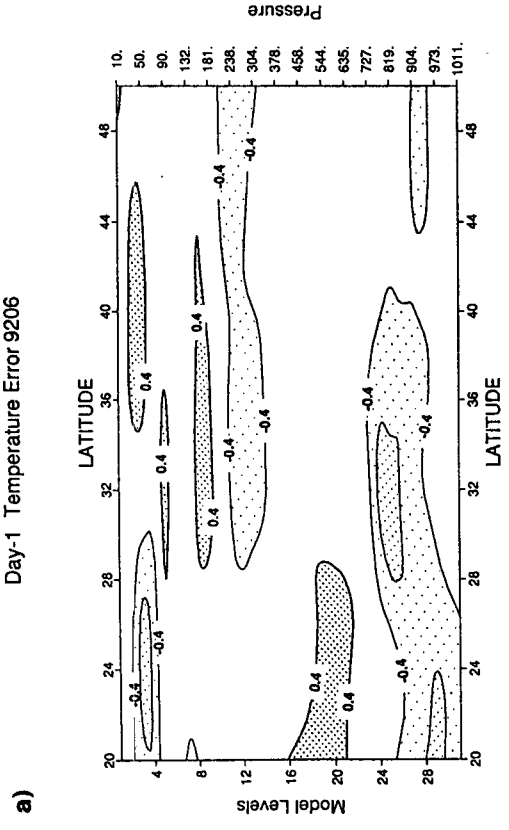

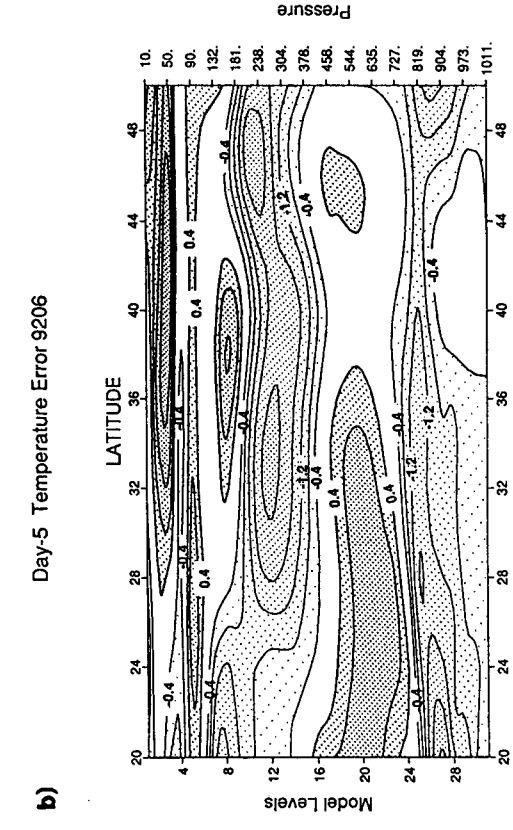

FIG. 14. Monthly (a) day 1 and (b) day 5 mean forecast temperature errors for June 1992.

though the ECMWF analyses seemed to quite accurately capture much of the sounding variability at the ceilometer sites. This suggested that the principal problem may have been the cloud parameterization itself. We tested this directly by applying the ECMWF algorithm [Eq. (3)] to predict inversion cloud fraction based on the actual soundings rather than the analyzed soundings.

To do this comparison we used only soundings with identifiable inversions, in which potential temperature increased by 1.5 K over 10 hPa (this constituted 88%, 98%, and 86% of all soundings at SM, PS, and VL with simultaneous ceilometer cloud measurements), and used the lowest such inversion for each sounding to define the inversion base pressure p_{ib}. Visual inspection showed that this automated criterion almost always isolated the proper trade inversion. The jump in potential temperature $\Delta\theta$ that goes into Eq. (3) for C_{Li} was taken to be the potential temperature difference over the 30-hPa interval from 10 hPa below p_{ib} to 20 hPa above p_{ib}.

The second row of Table 2 shows that the correlation between daily averaged C_{Li} and low cloudiness was negative at all stations and that difference in the mean C_{Li} between SM and PS was also opposite to the observed difference in mean low cloudiness. Large C_{Li} was clearly not a good predictor of large low cloud fraction in this region. Unlike the ECMWF-analyzed low cloud fractions, the mean C_{Li} deduced from sonde observations tended to be higher than the observed cloud fraction. This difference was mainly due to the stronger inversion in the observations than in the analyses. Other possible contributors to this difference include the finer pressure interval used for calculating the inversion stratification in the sonde analysis (30 hPa versus the approximately 40-hPa ECMWF model spacing) and the removal of soundings with no inversion from the sonde analysis.

b. *Other diagnostic parameterizations*

From the radiosonde soundings, we calculated a number of other quantities that have been hypothesized to be tied to boundary-layer cloudiness. The inversion strength $\Delta\theta_v$ (the inversion jump of virtual potential temperature, defined analogously to $\Delta\theta$ of the previous section) is nearly proportional to the ECMWF C_{Li}; the hypothesis was that stronger $\Delta\theta_v$ is correlated with more low cloud. MacVean (1993) defined a cloud-top entrainment parameter $R = C_p\Delta\theta_e/L\Delta q_t$. ($C_p\Delta\theta_e$ and $L\Delta q_t$ are normalized temperature and mixing ratio jumps across the trade inversion.) He showed that in an idealized numerical model calculation, a layer cloud with high cloud fraction cannot be supported with values of $R > 0.7$ and that mean cloud fraction tends to decrease when R exceeds 0.4. This suggests that R should be negatively correlated with cloud fraction; $1 - R$ can also be regarded as a surrogate for the MBL average mixing-line slope $-d\theta/dq_v$ between the surface and the inversion top, since the changes in θ and q_v within the MBL tend to be smaller than the inversion jumps. Betts and Boers (1990) found an empirical correlation between smaller mixing-line slope (larger R) and less MBL cloud. Klein and Hartmann (1993) showed that on seasonal or longer timescales regional and temporal variations of lower tropospheric stability $S = \theta(700\text{ hPa}) - \text{SST}$ are highly correlated with variations in marine stratocumulus cloud amount. By enhancing surface heat fluxes, stronger cold advection $\mathbf{u}\cdot\nabla(\text{SST})$ may promote vertical convective mixing that can serve as a moisture source for clouds. In the ASTEX region, the SST gradient is approximately from north to south (Albrecht et al. 1994, Fig. 13a) and of similar magnitude at all three ceilometer sites, so the northerly wind component $-v$ was used as a surrogate for $\mathbf{u}\cdot\nabla(\text{SST})$. We might also expect boundary-layer relative humidity and mean vertical motion to correlate positively with cloud amount. We do not expect these sounding parameters (except perhaps relative humidity) to have much correlation with the diurnal cycle of cloud, so we restrict our attention to synoptic-scale variability in cloud fraction by comparing daily averages.

The third and following rows in Table 2 show the correlation between daily average ceilometer cloud fraction and a suite of sounding-derived parameters at the ASTEX ceilometer sites; each averaged over all soundings on a given day. The parameter means and

TABLE 2. Correlation of daily average of sounding parameters with daily averaged ceilometer low cloud fraction (parameter mean and standard deviations in parentheses). Single and double asterisks indicates correlations significant at the 95% and 99% levels for a two-sided test, assuming all days are statistically independent.

Parameter	SM (4–23 June)	PS (1–25 June)	VL (6–14 June)
Low cloud fraction	(68 ± 28%)	(52 ± 17)	(40 ± 13)
C_{Li} (Δp = 30 hPa)	−0.51* (64 ± 27)	−0.33 (77 ± 18)	−0.02 (79 ± 19)
$\Delta\theta_v$	−0.54* (4.8 ± 0.9 K)	−0.04 (5.2 ± 1.4)	0.33 (5.3 ± 1.3)
$S = \theta(700\text{ hPa}) - \text{SST}$	−0.41 (16.9 ± 1.3 K)	0.34 (16.8 ± 1.4)	0.17 (18.4 ± 2.5)
$R = C_p\Delta\theta_e/L\Delta q_t$	−0.43 (0.21 ± 0.24)	0.06 (0.26 ± 0.15)	−0.34 (0.32 ± 0.07)
$-v$ ($\approx\mathbf{u}\cdot\nabla(\text{SST})$)	0.47* (4.3 ± 2.7 m s^{-1})	0.04 (6.6 ± 2.3)	0.23 (4.9 ± 1.2)
ω(850 hPa)	−0.54* (0.02 ± 0.02 Pa s^{-1})	0.13 (0.03 ± 0.02)	0.03 (0.04 ± 0.02)
p_{ib}	0.27 (875 ± 41 hPa)	−0.05 (841 ± 31)	0.42 (871 ± 15)
RH_{UCL}	0.80** (82 ± 12%)	0.50* (79 ± 12)	0.54 (79 ± 12)

standard deviations at each site are also tabulated, so that sites can be compared. Since there were only nine days of data at the *Valdivia,* the correlations there were quite uncertain statistically. Even for the other stations, only the strongest correlations can be expected to stand out in only 20–25 days of data. A longer record would be preferable for doing this type of analysis. For the parameters $\Delta\theta_v$, R, and S, the sign of the correlation coefficient was different at different stations. The negative correlation of $\Delta\theta_v$ at SM is barely statistically significant at the 95% level but does not hold up at the other stations. The correlation of cold advection $-v$ with cloudiness did have the expected sign at all stations but was large only at SM. Upward mean 850-hPa vertical velocity was correlated at the 95% level with cloud at SM (which felt the influence of the south end of several frontal systems), but the correlation had the reverse sign and small magnitude at the other two sites. Low inversion height (high inversion base pressure p_{ib}) was not significantly correlated with low cloud fraction at any site.

We can also see if intersite differences in the mean low cloud fraction correlate with variations in the mean values of these sounding parameters in the predicted way. The VL mean cloudiness is the lowest, but VL does not have the lowest mean C_{Li}, $\Delta\theta_v$, S, p_{ib}, or $-v$ of the three stations. However, the mean R does systematically increase from SM to PS to VL, tracking the cloudiness decrease in qualitative agreement with MacVean (1993) and Betts and Boers (1990).

The one variable tested that showed a consistent and sizable correlation with temporal variations of low cloud fraction at all three sites was the vertically averaged relative humidity RH_{UCL} over the upper half of the "cumulus" layer. The cumulus layer was defined to extend from the lifted condensation level of air at 1000 hPa to the inversion base p_{ib}. To a large extent, this correlation simply reflects the fact that cloud forms where the relative humidity is 100%. Albrecht (1981) also found this correlation using a much smaller set of cloud measurements and cloud reports from ship observers. Later, Albrecht (1991) reanalyzed this dataset and found, consistent with our study, that his results did not support MacVean's cloud breakup hypothesis.

5. Conclusions

We have extensively compared ECMWF analyses of the vertical thermodynamic structure and cloudiness in a midoceanic subtropical marine boundary layer with sounding, ceilometer, and satellite data from ASTEX. The results show that remarkable progress has been made over the last few years in better analyzing and forecasting MBL thermodynamic structure, but that the same cannot be said of MBL cloudiness. We found that in the ASTEX area ECMWF-predicted low cloud fraction was 0.2–0.3 less than both ceilometer and satellite-derived low cloud fraction and was completely uncorrelated with daily averaged ceilometer low cloud fraction at any of the three ASTEX ceilometer sites. We then tried to analyze some factors that might contribute to this lack of skill.

We found that the ECMWF analyses quite accurately represented the MBL vertical structure and its variability. During the ASTEX experiment most of the soundings taken were assimilated into the ECMWF operational model, to produce as accurate as possible a regional analysis in support of other ASTEX observations. Thus, the observed soundings should agree well with the analyses. However, this is a more stringent test than it seems. Only information from the standard levels of the soundings is assimilated, so the forecast model must supply the finer-resolution vertical structure that is crucial to the MBL. The analyses captured the temporal variability in soundings time series quite well, even at pressure levels not used for the assimilation. The systematic biases in the analysis were quite small, with small dry and warm biases in the upper part of the boundary layer and even smaller reverse biases above. These resulted in a 5%–10% underestimate of relative humidity beneath the inversion and tended to weaken the inversion. In 1- and 5-day forecasts somewhat different biases appeared, with a 40-hPa deepening of the inversion and moistening near the surface. These biases may have been promoted by the extremely strong feedback between cloudiness and inversion strength in the ECMWF low cloud scheme and may also have been related to the shallow convection scheme. These biases also suggest that the overall radiative cooling near the top of the boundary layer may already be overestimated in the model, even though low cloudiness is greatly underestimated. One possible cause of such errors would be an underestimate of cloud liquid water path, which would produce insufficient shortwave absorption in the clouds. This seems unlikely, since the liquid water mixing ratios assumed by the ECMWF cloud scheme (0.5 g kg^{-1} or larger at the temperatures of typical ASTEX clouds) are quite generous compared to ASTEX aircraft observations (e.g., Bretherton and Pincus 1994), and the ECMWF cloud thickness must be at least the vertical grid spacing, which is 30–40 hPa between 800 and 900 hPa. This cloud thickness is also large compared to the typical observed stratocumulus cloud thicknesses of 100–300 m observed in ASTEX. Thus, one would expect the ECMWF cloud liquid water path to be larger than observed. Vertical differencing and interpolation necessary to get heating rates at model levels may also generate large errors at a sharp inversion. Further investigation is required to distinguish between the possible sources of error.

Nevertheless, even in 5-day forecasts (during which a completely new airmass had moved into the ASTEX region) the overall MBL structure was qualitatively preserved. Both the analyses and forecasts suggested that the vertical structure of the MBL was represented

well enough in the ECMWF model to have some hope of predicting cloud fraction.

However, even when applied directly to the observed soundings, the ECMWF low cloud scheme could not predict the observed cloudiness variations at individual sites or the variation of mean cloudiness between the sites. Several other proposed diagnostic measures of low cloud fraction were tested and did not have statistically significant skill either. The only exception was relative humidity in the upper part of the boundary layer. This suggests that parameterizations that directly tie cloudiness to the MBL moisture sounding and the processes that drive it (e.g., shallow convection) have more chance to provide skillful prediction of day-to-day variation of cloud properties than parameterizations based on inversion jumps. For this type of parameterization, the 5%–10% low bias in relative humidity in the upper MBL could cause a substantial reduction in cloudiness. Given sufficient vertical resolution and an adequate initialization scheme, prognostic schemes for cloud liquid water and cloud fraction may be the best approach to a better depiction of the MBL vertical moisture structure. One such parameterization (Tiedtke 1993) is currently being tested at ECMWF.

Acknowledgments. This work was partly supported by ONR Grants N00014-90-J-1136 and N00014-90-J-1480. A. K. Betts was supported by NASA under Contract NAS5-31738 and NSF under Grant ATM9001960. Much of the work occurred while C. Bretherton and A. Betts were visiting scientists at ECMWF. Ceilometer and radiosonde data were provided by Dr. G. Kruspe of the Max-Planck-Institut, Hamburg, Germany (R/V *Valdivia*); W. Syrett and Dr. B. Albrecht of The Pennsylvania State University (Santa Maria); and Drs. S. Cox and W. Schubert of Colorado State University. Without the help of Dr. Carlos Tavares and several skilled GTS keypunchers from INMG in Lisbon, the ASTEX soundings would not have been assimilated into the ECMWF model. Steve Klein and Robert Pincus provided useful editorial suggestions.

REFERENCES

Albrecht, B. A., 1981: Parameterization of trade-cumulus cloud amount. *J. Atmos. Sci.*, **38,** 97–105.

——, 1991: Fractional cloudiness and cloud-top entrainment instability. *J. Atmos. Sci.*, **48,** 1519–1525.

——, C. S. Bretherton, and D. Johnson, 1994: The Atlantic Stratocumulus Transition Experiment (ASTEX). *Bull. Amer. Meteor. Soc.*, **76,** 889–904.

Betts, A. K., and R. Boers, 1990: A cloudiness transition in a marine boundary layer. *J. Atmos. Sci.*, **40,** 1480–1497.

Bretherton, C. S., and R. Pincus, 1995: Cloudiness and marine boundary layer dynamics in the ASTEX Lagrangian experiments. Part I: Synoptic setting and vertical structure. *J. Atmos. Sci.*, **52,** 2707–2723.

Cahalan, R. F., W. Ridgway, W. J. Wiscombe, and T. L. Bell, 1994: The albedo of fractal stratocumulus clouds. *J. Atmos. Sci.*, **51,** 2434–2455.

Coakley, J. A., and F. P. Bretherton, 1982: Cloud cover from high resolution scanner data; detecting and allowing for partially filled fields of view. *J. Geophys. Res.*, **87,** 4917–4932.

ECMWF, 1991: *Research Manual 3. ECMWF Forecast Model Physical Parameterization.* 3d ed. ECMWF Research Department, 140 pp.

Hartmann, D. L., M. E. Ockert-Bell, and M. L. Michelsen, 1992: The effect of cloud type on the earth's energy balance. *J. Climate,* **5,** 1281–1304.

Klein, S. A., and D. L. Hartmann, 1993: The seasonal cycle of low stratiform clouds. *J. Climate,* **6,** 1587–1606.

Klinker, E., and P. Sardeshmukh, 1992: The diagnosis of mechanical dissipation in the atmosphere from large-scale balance requirements. *J. Atmos. Sci.*, **49,** 608–627.

Kobayashi, T., 1993: Effects due to cloud geometry on biases in the albedo derived from radiance measurements. *J. Climate,* **6,** 120–128.

Li, Z.-X., and H. Le Treut, 1992: Cloud-radiation feedbacks in a general circulation model and their dependence on cloud modelling assumptions. *Climate Dyn.*, **7,** 133–140.

MacVean, M. K., 1993: A numerical investigation of the criterion for cloud-top entrainment instability. *J. Atmos. Sci.*, **50,** 2481–2495.

Minnis, P., P. W. Heck, D. F. Young, C. W. Fairall, and J. B. Snider, 1992: Stratocumulus cloud properties derived from simultaneous satellite and island-based instrumentation during FIRE. *J. Appl. Meteor.*, **31,** 317–339.

Rozendaal, M. A., C. B. Leovy, and S. A. Klein, 1994: An observational study of diurnal variations of marine stratiform cloud. *J. Climate,* in press.

Slingo, J. M., 1987: The development and verification of a cloud prediction scheme for the ECMWF model. *Quart. J. Roy. Meteor. Soc.*, **113,** 899–927.

Smith, R. N. B., 1990: A scheme for predicting layer clouds and their water contents in a general circulation model. *Quart. J. Roy. Meteor. Soc.*, **116,** 435–460.

Stephens, G. L., 1988: Radiative transfer through arbitrarily shaped optical media. Part I: A general method of solutions. *J. Atmos. Sci.*, **45,** 1818–1836.

Tiedtke, M., 1989: A comprehensive mass flux scheme for cumulus parmeterization in large-scale models. *Mon. Wea. Rev.*, **117,** 1779–1800.

——, 1993: Representation of clouds in large-scale models. *Mon. Wea. Rev.*, **121,** 3040–3061.

Welch, R., and B. A. Wielicki, 1985: A radiative parameterization of stratocumulus cloud fields. *J. Atmos. Sci.*, **42,** 2888–2897.